JOURNAL OF GEOPHYSICAL RESEARCH, VOL. 104, NO. D17, PAGES 21,503–21,512, SEPTEMBER 20, 1999

On the use of regularization techniques in the inverse modeling of atmospheric carbon dioxide

Song-Miao Fan and Jorge L. Sarmiento
Atmospheric and Oceanic Sciences Program, Princeton University, Princeton, New Jersey

Manuel Gloor and Stephen W. Pacala
Department of Ecology and Evolutionary Biology, Princeton University, Princeton, New Jersey

Abstract. The global distribution of carbon sources and sinks is estimated from atmospheric CO_2 measurements using an inverse method based on the Geophysical Fluid Dynamics Laboratory SKYHI atmospheric general circulation model. Applying the inverse model without any regularization yields unrealistically large CO_2 fluxes in the tropical regions. We examine the use of three regularization techniques that are commonly used to stabilize inversions: truncated singular value decomposition, imposition of a priori flux estimates, and use of a quadratic inequality constraint. The regularization techniques can all be made to minimize the unrealistic fluxes in the tropical regions. This brings inversion estimated CO_2 fluxes for oceanic regions in the tropics and in the Southern Hemisphere into better agreement with independent estimates of the air-sea exchange. However, one cannot assume that stabilized inversions give accurate estimates, as regularization merely holds the fluxes to a priori estimates or simply reduces them in magnitude in regions that are not resolvable by observations. By contrast, estimates of flux and uncertainty for the temperate North Atlantic, temperate North Pacific, and boreal and temperate North American regions are far less sensitive to the regularization parameters, consistent with the fact that these regions are better constrained by the present observations.

1. Introduction

Fossil fuel combustion, cement manufacture, and deforestation have released a large amount of CO_2 into the atmosphere and have caused atmospheric concentrations of CO_2 to rise from 280 parts per million (ppm) by volume before the Industrial Revolution to over 360 ppm today. On average the atmospheric increase of CO_2 accounts for 56% of the global CO_2 emissions from fossil fuel consumption and cement manufacture from 1959 to the present, implying that the combined oceanic and terrestrial uptake must account for 44% of the fossil CO_2 emissions [*Keeling et al*., 1995]. Uptake of anthropogenic CO_2 by the oceans and the terrestrial biosphere has been important in moderating the rate of CO_2 increase and, consequently, the pace of anthropogenic climate change due to the greenhouse effect of CO_2. The purpose of this study is to examine inverse modeling and regularization techniques that are used to estimate the spatial distribution of the net terrestrial and oceanic CO_2 sources and sinks.

Previously, measurements of atmospheric CO_2 have been combined with three-dimensional atmospheric transport models to infer surface CO_2 sources and sinks over the globe. The common strategy is to estimate an optimal combination of sources and sinks that allows atmospheric models to give the best prediction of the observed CO_2 patterns, either by trial and error [*Keeling et al*., 1989; *Tans et al*., 1990] or by linear least squares regression based on the singular value decomposition (SVD) method [*Enting et al*., 1995]. These studies agree on the magnitude of a large Northern Hemispheric carbon sink but disagree on its distribution between land biota and oceans and even more so on its distribution among the continents. Most recently, *Fan et al*. [1998] combined the method of linear least squares regression with the use of model and observational data of the air-sea CO_2 exchange and estimated terrestrial net ecosystem exchange of CO_2 for a small number of source regions.

Given the present data constraint, it is tempting to estimate CO_2 fluxes for boreal and temperate biomes separately in both Eurasia and North America and to estimate air-sea CO_2 exchange fluxes that are independent of oceanic observations and ocean model predictions. However, estimation of a large number of CO_2 source parameters may be obscured owing to a lack of observational data compounded by model errors. A Bayesian approach using prior flux estimates as additional constraints was followed by *Enting et al*. [1995] to prevent spurious estimates. In this study we attempt to estimate oceanic as well as land biotic CO_2 fluxes from 17 regions using singular value decomposition and to explore at the same time the use of three regularization techniques for damping spurious fluxes for regions poorly constrained by data: (1) inversion with a quadratic inequality constraint, (2) Bayesian inversion using a priori flux estimates, and (3) the truncation of singular values. The inverse model and the regularization techniques are described in section 2. The atmospheric CO_2 observations are described in section 3, followed by a description of the atmospheric models in section 4. Inverse modeling results are presented in section 5 and discussed in section 6. A summary of results and conclusions follows in section 7.

Paper number 1999JD900215.
0148-0227/99/1999JD900215$09.00

2. SVD-Based Inversion Method

Regional CO_2 fluxes over a period of several years may be estimated from the spatial patterns of atmospheric CO_2 that

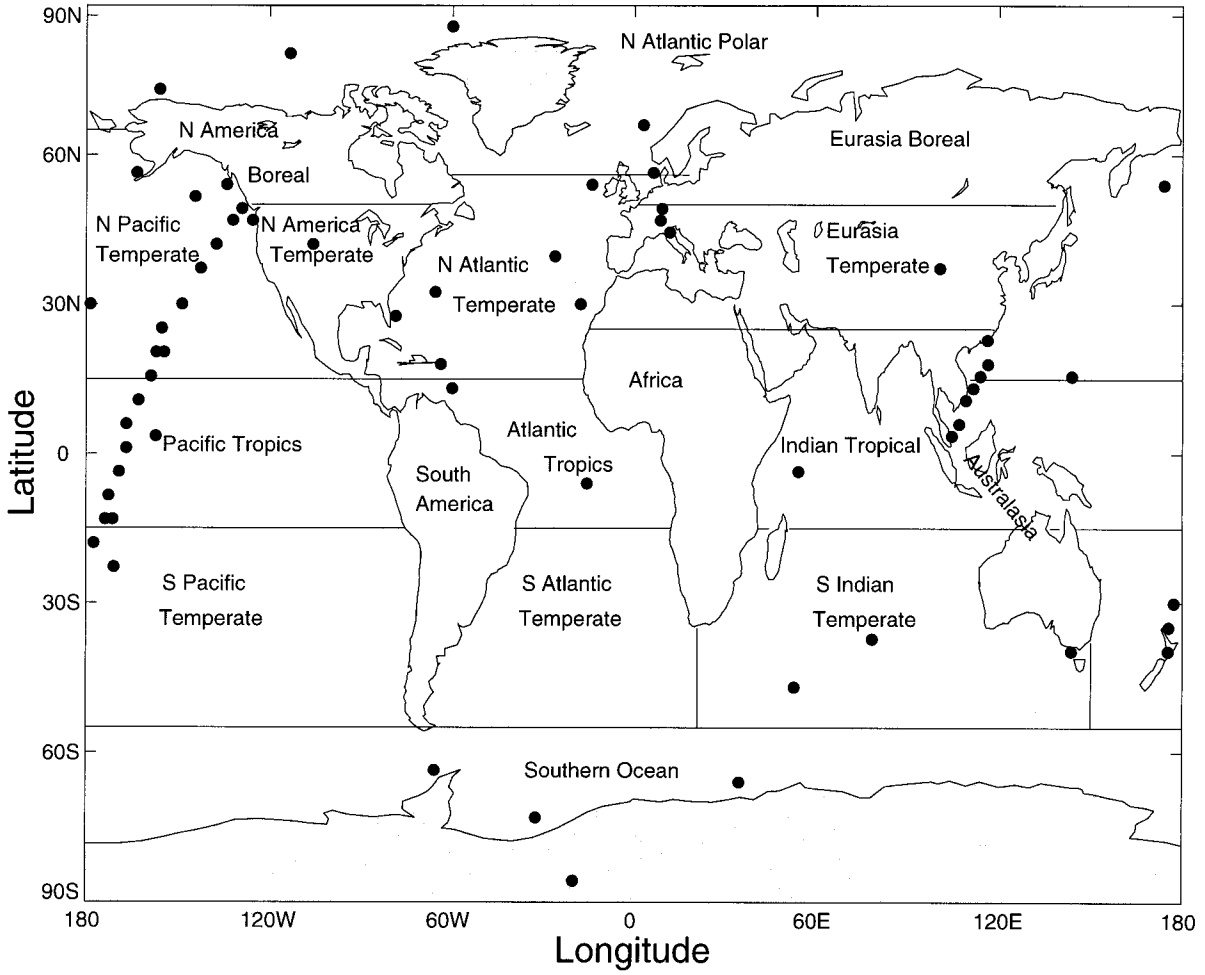

Figure 1. A map of the source regions. The locations of the atmospheric air sampling sites are indicated by solid circles.

result from net surface exchange and atmospheric transport. Spatial variations of atmospheric CO_2 result from fossil emissions, terrestrial net ecosystem productivity (NEP), air-sea exchanges of CO_2, and the oxidation of atmospheric CH_4 and CO. Terrestrial NEP may be separated into two components; one that is seasonally variable but averages to zero over an annual cycle and another that represents a net biome production over years. The contributions to atmospheric CO_2 of fossil CO_2 emissions and the seasonal NEP are calculated based on previous flux estimates. Annual terrestrial NEP and net air-sea CO_2 fluxes are estimated here by inverse modeling of atmospheric CO_2 observed over a 5 year period between 1988–1992 (see section 3). Independently obtained estimates of the air-sea CO_2 fluxes are used for testing the inverse modeling method. The oxidation of atmospheric CH_4 and CO are neglected.

The number of observations in the present sampling network are inadequate to constrain a large number of sources [*Gloor et al.*, 1999]. We aggregate the terrestrial ecosystems into seven source regions approximately according to biome distributions (Figure 1); subregional variations are smoothed out by the time air travels to the remote marine locations where most observations are made. We divide the global ocean into 10 oceanic source regions according to the ocean circulation features that are responsible for the spatial pattern of air-sea fluxes (Figure 1). Annual average fluxes will be estimated here for the seventeen carbon sources.

The mass conservation equation for atmospheric CO_2, which describes the balance between transport flux divergence and sources minus sinks, is linear in CO_2 concentration. The conservation equation for total CO_2 can thus be split into a set of equations for each of the CO_2 components, which allows us to model the source-specific components separately in a tracer model. On the basis of this premise, the steady state CO_2 concentration at any location $\vec{\mathbf{x}} = (x, y, z)$, given here as the difference between that site and the South Pole (for both model results and observations), can be represented as the sum

$$C(\vec{\mathbf{x}}) = C_{FF}(\vec{\mathbf{x}}) + C_{BB}(\vec{\mathbf{x}}) + \sum_{j=1}^{N} C_j(\vec{\mathbf{x}}) \qquad (1)$$

In this equation, $C_{FF}(\vec{\mathbf{x}})$ is the CO_2 concentration that results from fossil CO_2, $C_{BB}(\vec{\mathbf{x}})$ results from the seasonal NEP of the annually balanced biosphere (see below), and $C_j(\vec{\mathbf{x}})$ is caused by a net flux from the jth source region. The relationship of each of these concentrations to the corresponding source is predicted by specifying the surface flux and by integrating the mass conservation equation in an atmospheric general circu-

lation model (GCM). A quasi-steady state response is obtained after five years of model integration. Annual mean model results are obtained by averaging across the fifth year of model simulations. For proper comparison, CO_2 observations must be averaged over a period of multiple years to obtain a quasi steady state spatial distribution, as the influence by transient and interannual variations are minimized.

The fossil CO_2 flux is based on the 1990 emission map of *Andres et al*. [1996]. The land biotic CO_2 flux is specified using monthly NEP as calculated by the Carnegie, Ames, and Stanford Approach (CASA) ecosystem model [*Potter et al*., 1993]. The CASA model specifies a zero net exchange over an annual cycle for each grid cell on the surface of the Earth. However, the land biotic CO_2 in the atmospheric boundary layer may not average to zero because of the coherent seasonal variations in terrestrial NEP and atmospheric transport [*Denning et al*., 1995; *Law et al*., 1996].

Emission from each of the N ($N = 17$) sources is first assumed to be spatially uniform and constant in time when three regularization techniques are compared. The spatiotemporal patterns of emission are then assumed to be proportional to net primary productivity (NPP) for land regions and to the air-sea CO_2 flux estimates of *Takahashi et al*. [1997] for oceanic regions. If the quasi steady state distribution of atmospheric CO_2 caused by a constant flux of 1 Pg C yr^{-1} from the jth region is $a_j(\vec{\mathbf{x}})$, then atmospheric CO_2 caused by a flux of f_j Pg C yr^{-1} from the jth source is $C_j(\vec{\mathbf{x}}) = f_j a_j(\vec{\mathbf{x}})$. We can write total CO_2 as follows:

$$C(\vec{\mathbf{x}}) = C_{FF}(\vec{\mathbf{x}}) + C_{BB}(\vec{\mathbf{x}}) + \sum_{j=1}^{N} f_j a_j(\vec{\mathbf{x}}) \tag{2}$$

The regional sources $\{f_j\}$ may be estimated from the observations of atmospheric CO_2 using the least squares method by finding the f_j values that minimize

$$\chi^2 = \sum_{i=1}^{M} \frac{1}{\sigma_i^2} \left[C_{\text{obs}}(\vec{\mathbf{x}}_i) - C_{FF}(\vec{\mathbf{x}}_i) - C_{BB}(\vec{\mathbf{x}}_i) - \sum_{j=1}^{N} f_j a_j(\vec{\mathbf{x}}_i) \right]^2 \tag{3}$$

where M is the number of measurements, $C_{\text{obs}}(\vec{\mathbf{x}}_i)$ is the observed mean CO_2 concentration deviation at the ith sampling site, and σ_i is the measurement uncertainty. Following *Enting et al*. [1995], we use a uniform measurement uncertainty of $\sigma = 0.3$ ppm and test the sensitivity to σ. A realistic estimate of σ should consider instrument noise, calibration offset, and temporal variability of atmospheric CO_2. In addition, residual error (root-mean-squares) of the linear regression is larger than σ due to biases in model transport and basis function. A set of normal equations for the least squares problem can be solved for the flux vector $\mathbf{f} = \{f_j\}$ by use of the SVD method [*Press et al*., 1992].

The flux-to-concentration matrix $\mathbf{A}$, with elements $a_j(\vec{\mathbf{x}}_i)$ and dimensions $M \times N$, may be written as a product of three matrices by the SVD:

$$\mathbf{A} = \mathbf{U} \cdot \mathbf{W} \cdot \mathbf{V} \tag{4}$$

where $\mathbf{U}$ (with dimensions M × M) and $\mathbf{V}$ (with dimensions N × N) are orthogonal matrices, and $\mathbf{W} = [\text{diag}(w_j)$ $(j = 1, N)]$ is a diagonal matrix whose elements are the singular values of $\mathbf{A}$. The pseudo-inverse of $\mathbf{A}$ is defined as

$$\mathbf{A}^{-1} = \mathbf{V} \cdot [\text{diag}(1/w_j)] \cdot \mathbf{U}^T \tag{5}$$

and the solution of the linear regression problem is given by

$$\begin{aligned} \mathbf{f} &= \mathbf{A}^{-1} \cdot (\mathbf{C}_{\text{obs}} - \mathbf{C}_{FF} - \mathbf{C}_{BB}) \\ &= \mathbf{V} \cdot [\text{diag}(1/w_j)] \cdot \mathbf{U}^T \cdot (\mathbf{C}_{\text{obs}} - \mathbf{C}_{FF} - \mathbf{C}_{BB}) \end{aligned} \tag{6}$$

where $\mathbf{C}_{\text{obs}}$, $\mathbf{C}_{FF}$, and $\mathbf{C}_{BB}$ are vectors of CO_2 concentrations. The variance in the estimate of $\{f_j\}$ is given by

$$\sigma^2(f_j) = \sum_{k=1}^{N} \left(\frac{V_{jk}}{w_k} \right)^2 \tag{7}$$

where V_{jk} values are elements of the $\mathbf{V}$ matrix [*Press et al*., 1992]. Note that the matrix $\mathbf{A}$ may be expanded in the number of rows to include additional constraints such as a priori fluxes (see below); the $\mathbf{U}$, $\mathbf{V}$, and $\mathbf{W}$ matrices and the variances of $\{f_j\}$ are then calculated using the expanded $\mathbf{A}$ matrix.

Given the current data of atmospheric CO_2, plain linear regression for N ($N = 17$) sources yields spurious estimates of $\{f_j\}$ (see below) because a lack of observations in Africa, South America, and the South Atlantic Ocean causes large error amplifications in these regions; that is, a small measurement error results in large errors in the estimated fluxes (Gloor et al., submitted manuscript, 1999).

Three regularization techniques are used here to stabilize the linear regression. The first technique is to minimize χ^2 in (3) subject to the quadratic inequality constraint

$$\sum_{j=1}^{N} f_j^2 \le \alpha^2 \tag{8}$$

where α^2 is a tunable parameter [*Golub and Van Loan*, 1990]. This constraint restricts admissible solutions to within the volume of a multidimensional sphere. Large unstable fluxes that are not supported by observations are thus excluded.

In the second approach to regularization, "Bayesian inversion," a cost function

$$I = \chi^2 + \sum_{j=1}^{N} \frac{1}{\lambda_j^2} (f_j - s_j)^2 \tag{9}$$

is constructed and minimized, where χ^2 is the same as shown in (3), λ_j is the a priori flux uncertainty and s_j is the a priori flux estimate for the jth source. Minimization of the cost function I seeks to estimate the $\{f_j\}$ that both minimizes residuals and does not stray far from $\{s_j\}$. The a priori flux uncertainty is not known and must be assumed. We use a uniform flux uncertainty for the terrestrial sources, and a uniform flux uncertainty for oceanic sources, and the oceanic flux uncertainty is half that of the terrestrial sources. We test sensitivity of the inversion to a terrestrial flux uncertainty ranging between 0.5 and 4 Pg C yr^{-1}.

The third regularization technique is the truncated singular value decomposition [*Hansen*, 1987, 1990; *Press et al*., 1992; *Brown*, 1995]. Equation (7) indicates that the smallest w_j elements cause largest amplification of measurement error. The truncated SVD sets $1/w_j = 0$ for the smallest w_j elements, thus eliminating contributions by those components (columns of $\mathbf{V}$) of the solution that are sensitive to measurement error. The number of columns of $\mathbf{V}$ that are not truncated will be called the "truncation parameter." The utility of the truncated SVD depends on the ability to trade a relatively small increase

in χ^2 for a large decrease in the sensitivity of the solution to measurement error [*Brown*, 1995].

In addition, a mass conservation constraint is used in all three of the regularization approaches above to represent the global CO_2 balance:

$$\sum_{j=1}^{N} f_j = E - \frac{\Delta C}{\Delta t} \tag{10}$$

where $\Delta C/\Delta t$ is the annual atmospheric storage rate and E is the global annual fossil CO_2 emission rate. For the period of 1988–1992 the global fossil CO_2 emission rate is 6.1 Pg C yr^{-1} [*Marland et al*., 1994], the mean atmospheric CO_2 increase rate is 2.8 Pg C yr^{-1} [*Conway et al*., 1994], and so a mean global carbon uptake rate of 3.3 Pg C yr^{-1} is required to balance the budget.

3. Atmospheric Observations

High precision measurements of atmospheric CO_2 have been made for air samples from ground stations and on ocean ships (Figure 1) by laboratories in several countries. A globally consistent measurement record for the period from 1979–1992, the *GLOBALVIEW-CO_2* [1996], was produced based on atmospheric CO_2 data accumulated at the Climate Monitoring and Diagnostic Laboratory (CMDL) for 42 ground stations and 24 ocean ship sampling locations (Figure 1). Data gaps at some locations were filled using the sum of a latitudinal marine boundary layer CO_2 reference and monthly observations of the difference between a station and the reference at the same latitude [*Masarie and Tans*, 1995]. Data were edited to remove periods of contamination by local sources so that the measurements are representative of hundreds of kilometers. All laboratories contributing to the GLOBALVIEW-CO_2 participated in an interlaboratory comparison of standard gases and agreed to within 1 ppm, with the majority of calibration differences being <0.5 ppm. Here we use mean CO_2 concentrations over a 5 year period from 1988–1992 from this data base; no measurements were made at a number of sampling sites for the earlier period from 1979–1987 in the database. We thus make use of as many data points as available while minimizing the use of extrapolated/interpolated data. (Note, however, the Sable Island data were not used in this study because the size of a calibration offset remains to be resolved. Including Sable Island causes an increase in the magnitude of the boreal North American source and the temperate North American sink each by 0.2–0.3 Pg C yr^{-1} (cf. Table 4 and section 6).)

4. Transport Models

Atmospheric transport is simulated in this study using the GFDL SKYHI model. SKYHI calculates tracer transport "online" as the winds and other weather parameters are calculated, and the winds vary from 1 year to the next. The climatology of SKYHI is described by *Hamilton et al*. [1995]. The radiative variables are updated every 4 hours, whereas the weather is predicted every 225 s in the model. SKYHI has 40 vertical levels extending from the surface to 80 km altitude, with the lower layers following surface topography. Ten to fifteen of the layers are in the troposphere. The version of SKYHI used in this study has a horizontal grid size of $3° \times 3.6°$ latitude by longitude. Subgrid-scale transport processes are parameterized in the form of horizontal and vertical diffusion coefficients. The vertical diffusion coefficient is proportional to the local wind shear and the second power of the mixing length and is a function of the moist bulk Richardson number [*Levy et al*., 1982]. If the vertical thermal gradient is diagnosed as being unstable, a rapid mixing is activated (Jerry Mahlman, private communication, 1996). This rapid mixing is consistent with atmospheric observations and leads to realistic simulation of radon-222 in the free troposphere as well as in the continental boundary layer.

Transport in SKYHI has also been evaluated using observations of krypton-85, SF_6, and $CFCl_3$ [*Denning et al*., 1999; S. Fan, unpublished results, 1997]. SKYHI simulates well the meridional gradient of the tracers. Compared to other tracer models, SKYHI tends to predict higher surface SF_6 concentrations near the sources. However, SKYHI agrees with observations of SF_6 in the marine boundary layer from the Northern Hemisphere to the Southern Hemisphere [*Denning et al*., 1999].

Inverse modeling is very sensitive to model transport. As a limited analysis of the sensitivity, we also estimate CO_2 sources and sinks using the GFDL global chemical transport model (GCTM) model. GCTM is an off-line tracer model and was previously described by *Mahlman and Moxim* [1978] and *Levy et al*. [1982]. A comparison of GCTM with SKYHI and other atmospheric models is given by *Denning et al*. [1999]. GCTM predicts a larger north-to-south decrease of fossil CO_2 than SKYHI (Figure 2) because GCTM has a slower vertical mixing.

5. Inverse Modeling Results

Figure 2 shows the 5 year mean CO_2 observations at the sampling sites (shown as differences from the South Pole reference). The observations are lower than the sum of model predicted fossil fuel CO_2 and the rectification of seasonal biospheric CO_2 by $\sim$2 ppm in the midlatitude Northern Hemisphere. A Northern Hemispheric carbon sink is thus needed to account for the difference. The predicted fossil CO_2 agrees with the model calculations of *Denning et al*. [1995], but our rectification CO_2 is lower than theirs in the midlatitude to high-latitude Northern Hemisphere. In the following we use the inverse model shown in (6) to estimate the magnitude of the carbon sources and sinks from the prescribed source regions (Figure 1).

Table 1 shows estimates of CO_2 flux obtained by the inverse model using the technique of least squares with a quadratic inequality constraint, with α^2 ranging from 22 to 3 (Pg C $yr^{-1})^2$ (this unit will be neglected hereafter). An α^2 of 22 is obtained from fluxes estimated without the regularization. The large terrestrial uptake in Africa, 1.9 Pg C yr^{-1}, is not supported by any data in the literature. Documented changes in land cover and land use are estimated to cause a net emission of CO_2 in tropical Africa (see *Houghton* [1996] and *Gaston et al*. [1998] for the most recent estimates). The tropical oceanic sources, totaling 3.2 Pg C yr^{-1}, are 4 times as much as estimated by *Takahashi et al*. [1997] (referred to as T97 hereafter) and 6 times that predicted by the Princeton ocean biogeochemistry model (OBM) [*Murnane et al*., 1999]. These spurious fluxes result because the data constraint is insufficient in the tropical regions and because CO_2 emitted by tropical sources is diluted to very low concentrations by rapid vertical mixing in the tropical troposphere [*Gloor et al*., 1999].

As α^2 is set to smaller values, the tropical land biosphere changes from a large carbon sink to a small carbon source, and

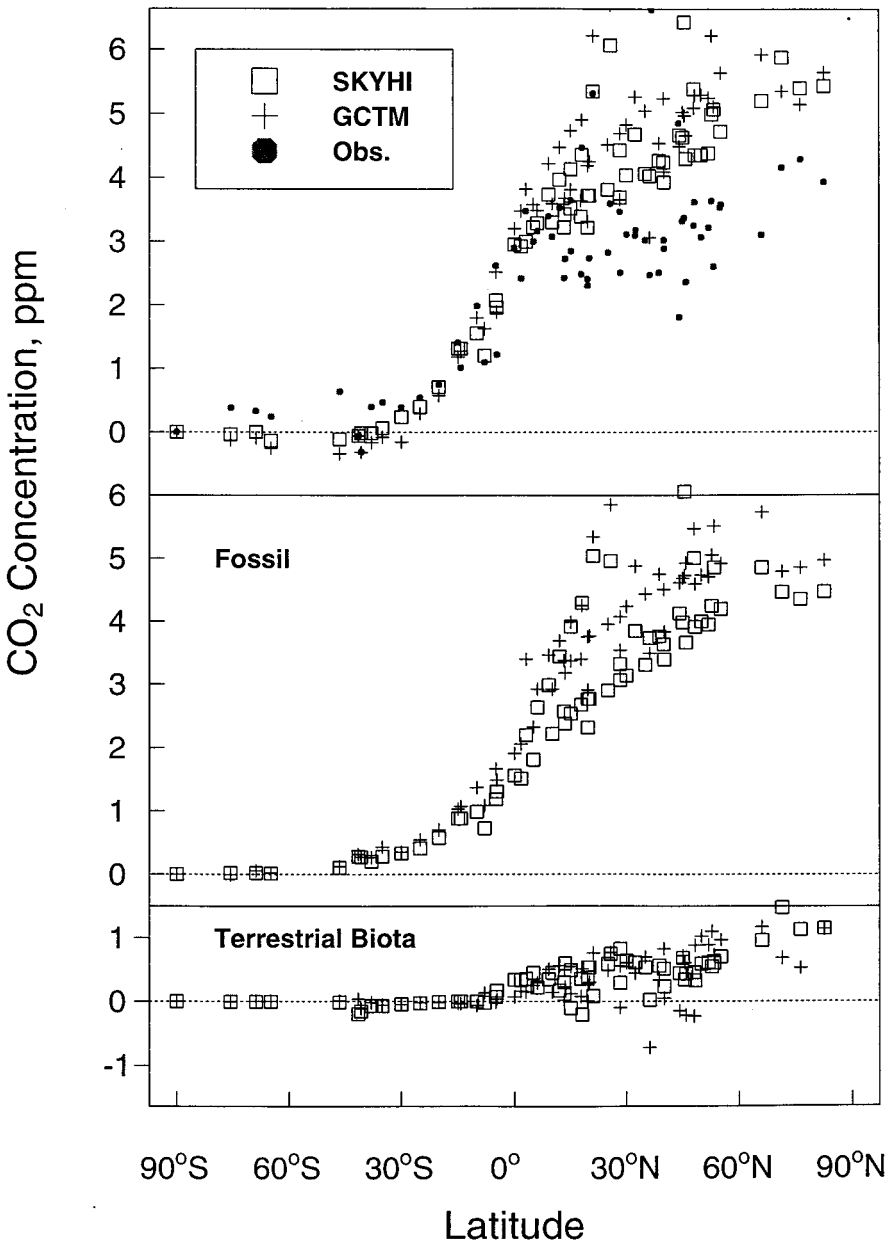

Figure 2. Atmospheric CO_2 at the sampling stations (given as differences from the South Pole reference). Station observations are given for the 5 year mean from 1988–1992. Fossil CO_2 and terrestrial biotic CO_2 are predicted by the models for fossil CO_2 emissions [*Andres et al.*, 1996] and seasonal net ecosystem productivity (with zero annual mean) calculated by the Carnegie, Ames, and Stanford Approach (CASA) model [*Potter et al.*, 1993], respectively.

the tropical oceans from an unrealistically large carbon source to a source more consistent with the independent estimates. The "goodness of fit" as measured by the root mean square (rms) of the residuals remains unchanged as α^2 ranges from 22 to 9, indicating that fluxes estimated with an α^2 of 9 fit the data as well as the unrestricted inverse modeling results. Therefore what the α^2 constraint does is force the flux estimates for regions with few data constraints to be small while maintaining a minimum χ^2. Any net ecosystem CO_2 exchanges in Africa and South America, which may exist but are not resolvable by the observations and are estimated incorrectly to be small with the regularization, may be forced to spread out to other regions to conserve mass.

For Northern Hemispheric regions with comparatively large data coverage, the inverse modeling results are not very sensitive to the value of α^2 (Table 1). These regions are boreal North America, temperate North America, temperate North Atlantic Ocean, and temperate North Pacific Ocean. The sum of boreal and temperate Eurasian fluxes remains constant with α^2 as well, although they are sensitive to α^2 separately. The sum of tropical and Southern Hemispheric regions is also well constrained by the data and the global mass balance. For small α^2 (≤ 6) the inverse modeling results are smeared to small values even for North American regions and for the Northern Hemisphere oceanic regions, and the rms error becomes larger.

Table 1. Carbon Fluxes Estimated for 1988–1992 by the Inverse Model With the Use of a Quadratic Inequality Constraint

	α^2							
Source Regions	22	15	12	9	6	3	T97	OBM
Boreal Eurasia	−1.6	−1.5	−1.4	−1.2	−0.9	−0.6		
Temperate Eurasia	1.1	0.9	0.7	0.5	0.3	0.0		
Subtotal	−0.5	−0.6	−0.6	−0.6	−0.7	−0.7		
Boreal North America	0.2	0.2	0.2	0.1	0.0	−0.2		
Temperate North America	−2.2	−2.1	−2.0	−1.9	−1.6	−1.0		
Subtotal	−2.0	−1.9	−1.8	−1.7	−1.5	−1.2		
Africa	−1.9	−0.6	−0.1	0.0	0.1	0.0		
South America	−1.2	−0.7	−0.3	−0.1	0.0	0.0		
Austral-Asia	1.1	1.1	0.9	0.6	0.4	0.1		
Subtotal	−1.9	−0.2	0.4	0.5	0.4	0.1		
Total terrestrial	−4.4	−2.7	−2.1	−1.9	−1.8	−1.8		
Polar North Atlantic	0.2	0.2	0.1	0.1	0.1	0.0	−0.3	−0.3
Temperate North Pacific	−0.1	−0.2	−0.2	−0.2	−0.3	−0.3	−0.3	−0.7
Temperate North Atlantic	−0.6	−0.7	−0.8	−0.8	−0.8	−0.7	−0.3	−0.3
Subtotal	−0.5	−0.7	−0.9	−0.9	−1.0	−1.0	−0.9	−1.2
Tropical Indian	0.2	0.1	0.2	0.2	0.2	0.2	0.1	0.0
Tropical Pacific	1.7	1.3	1.1	1.0	0.8	0.5	0.6	0.4
Tropical Atlantic	1.2	0.8	0.6	0.5	0.3	0.2	0.1	0.1
Subtotal	3.2	2.2	1.8	1.6	1.4	0.9	0.8	0.5
Temperate South Atlantic	−0.9	−1.0	−0.9	−0.7	−0.6	−0.3	−0.2	−0.2
Temperate South Indian	0.1	−0.1	−0.2	−0.3	−0.4	−0.3	−0.4	−0.5
Temperate South Pacific	−1.0	−1.1	−1.1	−0.9	−0.6	−0.4	−0.3	−0.5
Southern Ocean	0.2	0.2	0.1	−0.1	−0.2	−0.4	−0.1	−0.4
Subtotal	−1.6	−2.1	−2.2	−2.1	−1.8	−1.4	−1.0	−1.6
Total ocean	1.1	−0.6	−1.2	−1.4	−1.5	−1.5	−1.1	−2.3
rms error, ppm	0.46	0.47	0.47	0.47	0.48	0.52		

T97 is *Takahashi et al*., [1997]; OBM is Princeton ocean biogeochemistry model [*Murnane et al*., 1999]. Carbon fluxes are given in Pg C yr^{-1}. The quadratic inequality constraint is the sum of the fluxes squared is less than or equal to α^2.

Table 2 shows inverse modeling results when a priori fluxes were used as additional constraints for a range of a priori flux uncertainties (denoted hereafter by λ for terrestrial sources). The a priori oceanic fluxes are adopted from the T97 estimates, and the a priori terrestrial fluxes represent our initial guess. The a posteriori flux uncertainties are calculated as in (7). The a posteriori flux uncertainties increase proportionately with σ when no regularization is applied and approaches the a priori uncertainties as their magnitudes are decreased. For instance, when σ is increased from 0.3 to 0.6 ppm to account for additional error caused by the transport model and the basis functions, the a posteriori uncertainties for terrestrial fluxes were increased by approximately a factor of 2 and 1.5 for $\lambda = 4.0$ and 0.5 Pg C yr^{-1}, respectively. The Northern Hemisphere land and oceanic sources estimated by inverse modeling appear to be insensitive to λ between 0.5 and 4 Pg C yr^{-1}. The a posteriori uncertainties for these regions are much smaller than, and show minimal variations with, the a priori flux uncertainties. The fluxes estimated for the Northern Hemisphere sources do not appear to be shaped by the initial guesses and are hence really determined by the observations.

By contrast, the fluxes estimated for the tropical sources, particularly Africa and South America, vary strongly with λ; their a posteriori uncertainties show similar sensitivity and are relatively large in size (Table 2). The small reduction of uncertainty for Africa and South America indicate that these regions are only marginally constrained by the data. The sensitivities to the a priori flux uncertainties, which determine the relative weights given to the CO_2 observations and to the initial guesses, thus indicate the level of constraint. By this scale, the tropical and Southern Hemisphere oceans seem to be better constrained than the tropical lands, although they are not as well constrained as the northern oceans and North American regions. As more weight is given to the prior estimates (corresponding to smaller λ values in Table 2), the tropical sources are held closer and closer to the prior estimates.

The rms errors appear to be constant with λ in the range shown in Table 2. However, the rms error would increase as λ decreases if the a priori estimates were set to values far off from the inversion estimates shown in Table 2. This is because the inversion estimates would be held close to incorrect prior estimates at small λ values even for source regions where data constraints are strong.

Inversions using the truncated SVD are shown in Table 3. As before, the Northern Hemisphere land and oceanic regions are less sensitive to the regularization and better constrained by the observations than Southern Hemispheric regions and tropical regions. The northern sources are not sensitive to the truncation parameter from 16 to 12 and are similar to the results shown in Tables 1 and 2. Figure 3 shows the singular values ordered by magnitude from the largest to the smallest that are normalized by the largest singular value. There appear to be three groups of source components: The first 3–5 components are relatively well constrained, the components in the middle group are less constrained, and the last 3–5 components are least constrained. Zeroing out the last 3–5 components eliminates the spurious fluxes in the tropical regions while maintaining the "goodness of fit." However, some information provided by the observational data may be lost when too many components are truncated (see the last column of Table 3), which may result in erroneous flux estimates. Fluxes estimated for the tropical and Southern Hemisphere oceans

Table 2. Carbon Fluxes Estimated for 1988–1992 by the Inverse Model With the Use of a priori Flux and Uncertainty Constraints

Source Regions	a priori Fluxes	a priori Flux Uncertainties			
		4.0	2.0	1.0	0.5
Boreal Eurasia	−1.0	−1.6 ± 0.4	−1.5 ± 0.3	−1.5 ± 0.3	−1.4 ± 0.3
Temperate Eurasia	0	1.0 ± 0.6	0.9 ± 0.5	0.9 ± 0.4	0.7 ± 0.3
Subtotal	−1.0	−0.6	−0.6	−0.6	−0.7
Boreal North America	0	0.2 ± 0.2	0.2 ± 0.2	0.2 ± 0.2	0.2 ± 0.2
Temperate North America	−1.0	−2.2 ± 0.3	−2.2 ± 0.3	−2.2 ± 0.3	−2.1 ± 0.2
Subtotal	−1.0	−2.0	−2.0	−2.0	−1.9
Africa	0	−1.1 ± 2.1	−0.5 ± 1.4	0.0 ± 0.8	0.1 ± 0.4
South America	0	−1.1 ± 2.1	−0.8 ± 1.4	−0.3 ± 0.8	−0.1 ± 0.4
Austral-Asia	0	1.1 ± 0.7	1.0 ± 0.6	0.7 ± 0.5	0.4 ± 0.3
Subtotal	0	−1.1	−0.3	0.4	0.4
Total terrestrial	−2.0	−3.6	−2.7	−2.2	−2.1
Polar North Atlantic	−0.3	0.2 ± 0.2	0.2 ± 0.2	0.2 ± 0.2	0.1 ± 0.1
Temperate North Pacific	−0.3	−0.1 ± 0.2	−0.1 ± 0.2	−0.1 ± 0.2	−0.1 ± 0.2
Temperate North Atlantic	−0.3	−0.7 ± 0.3	−0.7 ± 0.3	−0.7 ± 0.2	−0.5 ± 0.2
Subtotal	−0.9	−0.5	−0.6	−0.7	−0.6
Tropical Indian	0.1	0.2 ± 0.4	0.1 ± 0.3	0.1 ± 0.3	0.2 ± 0.2
Tropical Pacific	0.6	1.6 ± 0.6	1.3 ± 0.5	1.0 ± 0.3	0.8 ± 0.2
Tropical Atlantic	0.1	1.0 ± 0.6	0.7 ± 0.4	0.4 ± 0.3	0.2 ± 0.2
Subtotal	0.8	2.7	2.1	1.6	1.2
Temperate South Atlantic	−0.2	−0.9 ± 0.8	−0.8 ± 0.6	−0.7 ± 0.4	−0.5 ± 0.2
Temperate South Indian	−0.4	−0.1 ± 0.5	−0.2 ± 0.4	−0.4 ± 0.3	−0.4 ± 0.2
Temperate South Pacific	−0.3	−1.0 ± 0.7	−1.0 ± 0.5	−0.8 ± 0.4	−0.5 ± 0.2
Southern Ocean	−0.1	0.2 ± 0.2	0.1 ± 0.2	−0.1 ± 0.2	−0.3 ± 0.1
Subtotal	−1.0	−1.8	−2.0	−2.0	−1.8
Total ocean	−1.1	0.3	−0.5	−1.1	−1.1
rms error, ppm		0.46	0.47	0.47	0.48

The a priori flux uncertainties are shown for the terrestrial sources; the values assumed for the oceanic sources are half as much as shown. The uncertainties for CO_2 observations are taken to be 0.3 ppm uniformly. Carbon fluxes are given in Pg C yr^{-1}.

show more variability with the truncation parameter. African and South American fluxes are again held to near zero by the regularization.

6. Discussion

The inverse modeling results for boreal and temperate North America and for temperate North Atlantic and North Pacific oceans appear to be least sensitive to regularization parameters, indicating that flux estimates for these regions are robustly constrained with the present observations. The air-sea CO_2 flux estimated for temperate North Pacific Ocean is smaller than the OBM prediction and the T97 estimates (Table 1), while that for temperate North Atlantic Ocean is ~2 times larger in magnitude than the OBM and T97 estimates. It is possible that the large North Atlantic sink represents a fraction of the North American sink misattributed by error in the inversions. The North American and North Atlantic regions are tightly coupled in the inverse model because they are both heavily constrained by atmospheric CO_2 observations in the North Atlantic region.

Variations of the inverse modeling results with the regularization parameters are found to compensate for each other between boreal and temperate regions of Eurasia and between the tropical regions and the Southern Hemisphere (Tables 1–3). These compensating variations indicate that the combined regions (boreal and temperate Eurasia, the tropics, and Southern Hemisphere) as a whole are better constrained by the observations than the separate components that make them up.

The inverse modeling results suggest an outgassing by tropical oceans, where upwelling brings CO_2-rich deep water to the surface, in agreement with observations. The tropical Pacific source is estimated to be of order 1 Pg C yr^{-1}, larger than the OBM result and the T97 estimate. More recent measurements suggest that the tropical Pacific source is as large as 1 Pg C yr^{-1} in non-El Nino years but small (≤0.5 Pg C yr^{-1}) in El Nino years [*Feely et al*., 1997].

A large CO_2 uptake is estimated for oceanic regions in the Southern Hemisphere as a whole; it ranges between 1.5 and 2.6 Pg C yr^{-1} (Tables 1–3). By comparison the total uptake by the temperate oceans and the Southern Ocean is estimated to be 1.0 Pg C yr^{-1} by T97 and 1.6 Pg C yr^{-1} by OBM. There exist considerable uncertainties in the T97 and OBM estimates. Measurements of pCO_2 are sparse in the Southern Hemisphere. Predicted ocean circulation and air-sea CO_2 exchange diverge among ocean models in the high-latitude Southern Hemisphere [*Sarmiento et al.,* 1999; J. C. Orr et al., manuscript in preparation, 1999]. The inverse modeling of atmospheric CO_2 provides an independent estimate for the air-sea CO_2 exchange that is in better agreement with OBM in the Southern Hemisphere (where fossil and biospheric CO_2 contributions are small). Further division of the sink among the regions is not resolvable by the sparse measurements in the Southern Hemisphere.

An alternative to the explicit use of regularization is to estimate a small number of sources that are resolvable by the data, although the spatial patterns must be assumed for even larger regions as a trade-off. In *Fan et al*. [1998], fluxes were estimated for three and four land regions while the sea-air fluxes were specified according to the OBM prediction or the

Table 3. Carbon Fluxes Estimated for 1988–1992 by the Inverse Model With the Use of Truncated Singular Value Decomposition

Source Regions	Truncation Parameter					
	16	15	14	13	12	9
Boreal Eurasia	−1.6	−1.5	−1.5	−1.6	−1.6	−0.9
Temperate Eurasia	1.1	0.7	0.8	1.2	1.1	−0.3
Subtotal	−0.5	−0.7	−0.7	−0.4	−0.5	−1.1
Boreal North America	0.2	0.3	0.3	0.2	0.2	0.0
Temperate North America	−2.2	−2.2	−2.2	−2.2	−2.2	−1.1
Subtotal	−2.0	−1.9	−1.9	−2.0	−2.0	−1.2
Africa	−1.6	0.2	0.2	0.3	0.3	0.1
South America	−1.6	−0.2	−0.2	0.0	0.0	0.1
Austral-Asia	1.1	1.3	1.1	0.5	0.7	−0.2
Subtotal	−2.0	1.3	1.1	0.8	1.0	0.1
Total terrestrial	−4.5	−1.4	−1.4	−1.6	−1.5	−2.2
Polar North Atlantic	0.2	0.1	0.1	0.2	0.2	0.1
Temperate North Pacific	−0.1	−0.2	−0.2	−0.2	−0.2	−0.2
Temperate North Atlantic	−0.6	−0.8	−0.9	−0.8	−0.8	−1.3
Subtotal	−0.5	−0.9	−1.0	−0.8	−0.8	−1.4
Tropical Indian	0.2	−0.1	−0.1	0.0	0.1	0.9
Tropical Pacific	1.8	1.1	1.0	1.0	0.9	0.9
Tropical Atlantic	1.1	0.6	0.6	0.3	0.3	0.5
Subtotal	3.2	1.5	1.6	1.4	1.3	2.3
Temperate South Atlantic	−0.8	−1.1	−1.3	−0.6	−0.7	−0.4
Temperate South Indian	0.0	−0.1	−0.1	−0.3	−1.0	−0.8
Temperate South Pacific	−0.9	−1.5	−1.4	−1.2	−0.6	−0.7
Southern Ocean	0.2	0.2	0.2	0.0	0.0	−0.2
Subtotal	−1.5	−2.6	−2.5	−2.2	−2.3	−2.0
Total ocean	1.2	−1.9	−1.9	−1.7	−1.8	−1.1
rms error, ppm	0.46	0.47	0.47	0.47	0.48	0.51

Truncation parameter is defined as the number of singular values that are not set to zero in the diagonal matrix in a singular value decomposition (SVD). Carbon fluxes are given in Pg C yr^{-1}.

T97 estimates. Land biomes were aggregated into Eurasia, North America as a whole or as separate boreal and temperate regions, and the rest of land regions as a whole that include South and Central Africa, Australia, South America, and tropical Asia. The net terrestrial source/sink assumed the same spatio-temporal patterns of NPP as predicted by the CASA model. A large North American carbon sink was estimated by *Fan et al*. [1998], which appears to be the most robust of all estimates in the three- or four-region inversions.

The large North American sink is estimated in all the 17-region inversions (Tables 1–3), even though the 17-region inversions use uniform and constant basis functions for all the oceanic and terrestrial sources and estimate the oceanic and terrestrial fluxes simultaneously. As a test of sensitivity to the basis function and transport model, Table 4 shows the CO_2 inversion for four combinations of tracer models (GCTM or SKYHI) and basis functions (NPP for terrestrial sources, T97 for oceanic sources, or flat for both terrestrial and oceanic sources). In all four inversions, boreal Eurasia, temperate North America, and the temperate oceans were found to be carbon sinks, while temperate Eurasia and boreal North America were found to be carbon sources. Although their magnitudes vary by as much as 1 Pg C yr^{-1} among the four combinations. Both the boreal sink in Eurasia and the temperate sink in North America appear to be significant given the range of variability (Table 4), although fewer measurements of CO_2 were made in the vicinity of boreal Eurasia than North America (Figure 1). In the tropics, no consistent source or sink fluxes were estimated for the land and oceanic regions except for the Pacific Ocean.

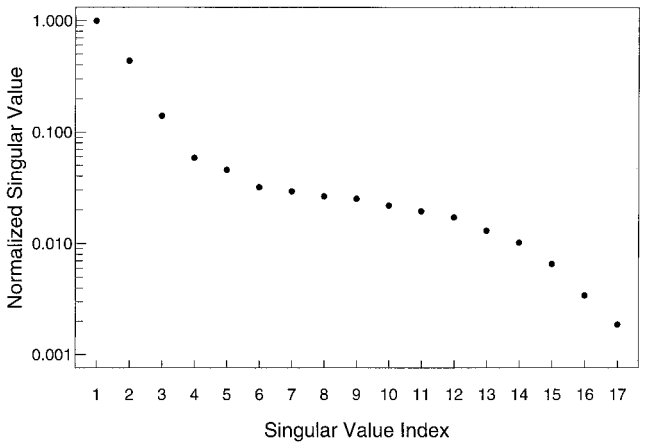

Figure 3. Singular values of the flux-to-concentration transformation matrix A based on SKYHI simulations for tracers with specified surface fluxes and normalized by the largest singular value.

A combination of factors are responsible for the differences between the inversions. Vertical mixing is primarily responsible for the difference between GCTM and SKYHI (see section 4). GCTM predicts a larger south-to-north gradient for fossil CO_2, thus implying a larger total uptake in the tropics and Northern Hemisphere and a smaller total uptake in the temperate Southern Hemisphere. The differences between inversions using NPP and inversions using flat basis functions are more complicated. Different CO_2 responses result from the coherent seasonal variations of NPP and transport (horizontal advection and vertical mixing) and a lack of seasonal variation

Table 4. A Comparison of Inversion Results for 1988–1992 and for Four Combinations of Tracer Models and Basis Functions

Source Regions	GCTM Flat	GCTM NPP, T97	SKYHI Flat	SKYHI NPP, Flat
Boreal Eurasia	−2.2 ± 0.4	−1.7 ± 0.4	−1.4 ± 0.4	−1.1 ± 0.4
Temperate Eurasia	0.9 ± 0.5	1.1 ± 0.6	0.8 ± 0.4	0.2 ± 0.4
Subtotal	−1.3	−0.6	−0.6	−0.9
Boreal North America	0.7 ± 0.3	0.9 ± 0.4	0.2 ± 0.2	0.1 ± 0.3
Temperate North America	−1.5 ± 0.3	−1.6 ± 0.3	−2.1 ± 0.3	−1.2 ± 0.2
Subtotal	−0.8	−0.7	−1.9	−1.1
Africa	0.8 ± 0.8	1.8 ± 0.7	0.0 ± 0.8	−0.2 ± 0.8
South America	−0.8 ± 0.7	0.3 ± 0.8	−0.4 ± 0.7	−0.2 ± 0.7
Austral-Asia	−0.3 ± 0.4	−1.9 ± 0.7	0.8 ± 0.5	1.5 ± 0.4
Subtotal	−0.3	0.2	0.4	1.1
Total terrestrial	−2.4	−1.1	−2.1	−0.9
Polar North Atlantic	0.0 ± 0.2	−0.2 ± 0.2	0.1 ± 0.2	−0.0 ± 0.1
Temperate North Pacific	−0.3 ± 0.2	−0.5 ± 0.2	−0.2 ± 0.2	−0.4 ± 0.2
Temperate North Atlantic	−0.7 ± 0.2	−0.7 ± 0.2	−0.7 ± 0.2	−0.8 ± 0.2
Subtotal	−1.0	−1.4	−0.8	−1.2
Tropical Indian	0.0 ± 0.2	−0.2 ± 0.2	0.1 ± 0.3	−0.3 ± 0.3
Tropical Pacific	1.2 ± 0.2	0.6 ± 0.2	1.1 ± 0.3	1.0 ± 0.3
Tropical Atlantic	0.3 ± 0.2	−0.3 ± 0.2	0.4 ± 0.3	0.4 ± 0.3
Subtotal	1.5	0.1	1.6	1.1
Temperate South Atlantic	−0.9 ± 0.4	−0.6 ± 0.3	−0.7 ± 0.4	−0.6 ± 0.4
Temperate South Indian	0.0 ± 0.3	0.0 ± 0.3	−0.5 ± 0.3	−0.4 ± 0.3
Temperate South Pacific	−0.3 ± 0.3	−0.1 ± 0.2	−0.9 ± 0.4	−1.0 ± 0.3
Southern Ocean	0.0 ± 0.2	−0.1 ± 0.2	0.0 ± 0.2	−0.1 ± 0.2
Subtotal	−1.2	−0.8	−2.1	−2.1
Total ocean	−0.7	−2.1	−1.3	−2.2

These inversions used a priori fluxes as additional constraints: zero for the terrestrial regions and *Takahashi et al*. [1997] (T97) estimates for oceanic regions. NPP is for land, Flat is for land, oceanic, or both. The a priori flux uncertainties used in the least squares regression are assumed to be 1 Pg C yr^{-1} for the terrestrial fluxes and 0.5 Pg C yr^{-1} for the oceanic fluxes. The uncertainties for CO_2 observations are taken to be 0.3 ppm uniformly. Flux is given in Pg C yr^{-1}.

in the uniform fluxes. The seasonal wind patterns differ between GCTM and SKYHI. Hence the change of CO_2 response from NPP to uniform fluxes is incoherent between the transport models at many sampling stations. As a consequence, the changes of inversion results from NPP to flat basis functions are not the same between GCTM and SKYHI.

Bayesian inversions constrained with a priori estimates have been reported for atmospheric CH_4 and CO_2 [*Enting et al*., 1995; *Hein et al*., 1997]. The truncated SVD method was used by *Brown* [1995] in her inverse modeling of atmospheric CH_4. The results presented in these studies must be evaluated against the observational constraints. The regularization techniques do not help to improve inversion estimates for parameters that are not constrained by data. A total of 26 sources was estimated from CO_2 observations at 21 sampling locations as given by *Enting et al*. [1995]. Such a system is severely underconstrained. The a posteriori uncertainties are reduced by less than 30% from the a priori estimates for most of the 26 sources. Ten types of methane sources and sinks were estimated by *Hein et al*. [1997]. About 50% reduction of uncertainty was obtained for some important methane sources (rice paddies, wetlands, and biomass burning). There is minimal reduction of uncertainty for half of the methane source/sink parameters, reflecting either an over-confident specification of the a priori uncertainties or a poorly constrained inversion.

7. Summary

We combined atmospheric observations of CO_2 from 1988 to 1992 with GFDL SKYHI atmospheric GCM to infer global sources and sinks of CO_2, using an SVD-based inverse modeling method. The inversion estimates are found to be spurious in the tropical regions and in the Southern Hemisphere where observations are sparse. Three regularization techniques were used to stabilize the inversions and are compared. These are the least squares with a quadratic inequality constraint, the Bayesian inversion that takes account of prior estimates, and the truncated SVD that zeros out contributions by unconstrained source components.

The CO_2 fluxes estimated by inverse modeling for the Northern Hemisphere regions are least sensitive to measurement errors and to regularization parameters. These regions appear to be best constrained by the atmospheric CO_2 observations. A comparison of air-sea fluxes estimated by inversion with ocean model predictions and with observation based estimates suggests that use of regularization can help improve inversion estimates for the tropical and Southern Hemisphere oceanic regions where observations are sparser than in the midlatitude Northern Hemisphere. However, inversions with regularization tend to hold the fluxes to a priori estimates for poorly constrained regions of Africa and South America. Reliable prior knowledge for, and observations in/near, these regions are obviously desirable.

This study qualitatively confirms the main results of *Fan et al*. [1998]. A large terrestrial uptake of CO_2 is suggested by the observations in temperate North America and also in boreal Eurasia (Tables 1–4). A Northern Hemisphere oceanic sink was estimated, most of which was attributed to the temperate North Atlantic Ocean. A tropical oceanic CO_2 source and a Southern Hemisphere oceanic sink were also estimated by the inversions. The latter was found to be mostly in the temperate

oceans, with only a small contribution by the Southern Ocean (south of 54°S).

Additional observations of atmospheric CO_2, the isotopic ratios of CO_2, and O_2, particularly from the tropics and the Southern Hemisphere, are needed to improve the estimation of CO_2 sources and sinks by inverse modeling. Optimal locations and sampling strategies for additional observations are the subject of a separate study [*Gloor et al*., 1999].

Acknowledgments. This study was carried out by the Carbon Modeling Consortium with support from the Office of Global Programs and Geophysical Fluid Dynamics Laboratory of the National Oceanic and Atmospheric Administration. The Globalview-CO_2 data was provided to us by P. Tans, the oceanic data was provided by T. Takahashi, the CASA model was provided by C. Field, and the SKYHI model was provided by J. Mahlman. L. Bruhwiler, R. Hemler, H. Levy, J. Mahlman, and W. Moxim provided advice on using the atmospheric models. Two anonymous reviewers are thanked for useful comments.

References

Andres, R. J., G. Marland, I. Fung, and E. Matthews, A 1° × 1° distribution of carbon dioxide emissions from fossil fuel consumption and cement manufacture, 1950–1990, *Global Biogeochem. Cycles*, *10*, 419–429, 1996.

Brown, M., The singular value decomposition method applied to the deduction of the emissions and the isotopic composition of atmospheric methane, *J. Geophys. Res*., *100*, 11,425–11,446, 1995.

Conway, T. J., P. P. Tans, L. S. Waterman, K. W. Thoning, D. R. Kitzis, K. A. Maserie, and N. Zhang, Evidence for interannual variability of the carbon cycle from the National Oceanic and Atmospheric Administration/Climate Monitoring and Diagnostics Laboratory global air sampling network, *J. Geophys. Res*., *99*, 22,831–22,855, 1994.

Denning, A. S., I. Y. Fung, and D. Randall, Latitudinal gradient of atmospheric CO_2 due to seasonal exchange with land biota, *Nature*, *376*, 240–243, 1995.

Denning, A. S., et al., Three-dimensional transport and concentration of SF_6: A model intercomparison study (TransCom 2), *Tellus*, *Ser. B*, *51 B*, 266–297, 1999.

Enting, I. G., C. M. Trudinger, and R. J. Francey, A synthesis inversion of the concentration and d13C of atmospheric CO_2, *Tellus*, *47B*, 35–52, 1995.

Fan, S., M. Gloor, J. Mahlman, S. Pacala, J. Sarmiento, T. Takahashi, and P. Tans, A large terrestrial carbon sink in North America implied by atmospheric and oceanic CO_2 data and models, *Science*, *282*, 442–446, 1998.

Feely, R. A., R. Wanninkhof, C. Goyet, D. E. Archer, and T. Takahashi, Variability of CO_2 distribution and sea-air fluxes in the central and eastern equatorial Pacific during the 1991–1994 El Niño, *Deep-Sea Res*., *Part II*, *44*, 1851–1867, 1997.

Gaston, G., S. Brown, M. Lorenzini, and K. D. Singh, State and change in carbon pools in the forests of tropical Africa, *Global Change Biology*, *4*, 97–114, 1998.

GLOBALVIEW-CO_2, *Cooperative Atmospheric Data Integration Project—Carbon Dioxide* [CD-ROM], Natl. Oceanic and Atmos. Admin/Clim. Monitoring and Diagnostics Lab, Boulder, Colo., 1996. (Also available via anonymous FTP to ftp.cmdl.noaa.gov, Path: ccg/co2/GLOBALVIEW.)

Gloor, M., S.-M. Fan, S. Pacala, and J. Sarmiento, Optimal sampling of the atmosphere for purposes of inverse modeling: A model, *Global Biogeochem. Cycles*, in press, 1999.

Golub, G. H., and C. F. Van Loan, *Matrix Computations*, Johns Hopkins Univ. Press, Baltimore, Md., 1990.

Hamilton, K., R. J. Wilson, J. D. Mahlman, and L. J. Umscheid, Climatology of the SKYHI troposphere-stratosphere-mesosphere general circulation model, *J. Atmos. Sci*., *52*, 5–43, 1995.

Hansen, P. C., The truncated SVD as a method for regularization, *BIT*, *27*, 534–553, 1987.

Hansen, P. C., Truncated singular value decomposition solutions to discrete ill-posed problems with ill-determined numerical rank, *SIAM J. Sci. Stat. Comput*., *11*, 503–518, 1990.

Hein, R., and P. J. Crutzen, An inverse modeling approach to investigate the global atmospheric methane cycle, *Global Biogeochem. Cycles*, *11*, 43–76, 1997.

Houghton, R. A., Terrestrial sources and sinks of carbon inferred from terrestrial data, *Tellus*, *Ser. B*, *48B*, 420–432, 1996.

Keeling, C. D., S. C. Piper, and M. Heimann, A three-dimensional model of atmospheric CO_2 transport based on observed winds: 4 Mea annual gradients and interannual variations, in *Aspects of Climate Variability in the Pacific and Western Americas*, *Geophys. Monogr. Ser*., vol. 55, edited by D. H. Peterson, pp. 305–363, AGU, Washington, D. C., 1989.

Keeling, C. D., T. P. Whorf, M. Wahlen, and J. van der Plicht, Interannual extremes in the rate of rise of atmospheric carbon dioxide since 1980, *Nature*, *375*, 666–670, 1995.

Law, R. M., et al., Variations in modeled atmospheric transport of carbon dioxide and the consequences for CO_2 inversions, *Global Biogeochem. Cycles*, *10*, 781–796, 1996.

Levy, H., II, J. D. Mahlman, and W. J. Moxim, Tropospheric N2O variability, *J. Geophys. Res*., *87*, 3061–3080, 1982.

Mahlman, J. D., and W. J. Moxim, Tracer simulation using a global general circulation model: Results from a mid-latitude instaneous source experiment, *J. Atmos. Sci*., *35*, 1340–1374, 1978.

Marland, G., R. J. Andres, and T. A. Boden, Global, regional, and national CO_2 emissions, in *Trends '93: A Compendium of Data on Global Change*, edited by T. A. Boden et al., *ORNL/CDIAC-65*, pp. 505–584, Carbon Dioxide Info. Anal. Cent., Oak Ridge Natl. Lab., Oak Ridge, Tenn., 1994.

Masarie, K. A., and P. P. Tans, Extension and integration of atmospheric carbon dioxide data into a globally consistent measurement record, *J. Geophys. Res*., *100*, 11,593–11,610, 1995.

Murnane, R. J., J. L. Sarmiento, and C. Le Quere, Spatial distribution of air-sea CO_2 fluxes and the interhemispheric transport of carbon by the oceans, *Global Biogeochem. Cycles*, in press, 1999.

Potter, C. S., et al., Terrestrial ecosystem production: A process model based on global satellite and surface data, *Global Biogeochem. Cycles*, *7*, 811–841, 1993.

Press, W. H., B. P. Flannery, S. A. Teukolsky, and W. T. Vetterling, *Numerical Recipes*, Cambridge Univ. Press, New York, 1992.

Sarmiento, J. L., et al., Sea-air CO_2 fluxes and carbon transport: A comparison of three ocean general circulation models, *Global Biogeochem. Cycles*, in press, 1999.

Takahashi, T., R. A. Feely, R. Weiss, R. H. Wanninkhof, D. W. Chipman, S. C. Sutherland, and T. Takahashi, Global air-sea flux of CO_2: An estimate based on measurements of sea-air pCO_2 difference, *Proc. Nat. Acad. Sci. U. S. A*., *94*, 8292–8299, 1997.

Tans, P. P., I. Y. Fung, and T. Takahashi, Observational constraints on the global atmospheric CO_2 budget, *Science*, *247*, 1431–1438, 1990.

S.-M. Fan and J. L. Sarmiento, Atmospheric and Oceanic Sciences Program, Princeton University, Sayre Hall/POB CN710, Princeton, NJ 08544. (fan@splash.princeton.edu)

M. Gloor and S. W. Pacala, Department of Ecology and Evolutionary Biology, Guyot Hall, Princeton, NJ 08544.

(Received September 8, 1998; revised March 30, 1999; accepted April 2, 1999.)